Theoretical Study of the Electronic Spectrum of Binuclear Gold(I) Complexes

FERNANDO MENDIZABAL,[1] CLAUDIO OLEA-AZAR[2]

[1]*Departamento de Química, Facultad de Ciencias, Universidad de Chile, Casilla 653, Santiago, Chile*

[2]*Departamento de Química Inorgánica y Analítica, Facultad de Ciencias Químicas y Farmacéuticas, Universidad de Chile, Casilla 233, Santiago 1, Chile*

ABSTRACT: The electronic structure and the spectroscopic properties of $[Au_2(CS_3)_2]^{-2}$, $[Au_2(pym\text{-}2\text{-}S)_2]$ (pym = pyrimidethiolate), $[Au_2(dpm)_2]^{+2}$ (dpm = bis(diphosphino)methane) were studied using density functional theory (DFT) at the B3LYP level. The absorption spectrum of these binuclear gold(I) complexes was calculated by single excitation time-dependent (TD) method. All complexes showed a $^1(5d\sigma^* \rightarrow 6p\sigma)$ transition associated with a metal–metal charge transfer, which is strongly interrelated with the gold–gold distance. Furthermore, we have calculated the frequency of the gold–gold vibration (ν_{Au2}) on the above complexes. The values obtained are theoretically in agreement with experimental range.

Key words: gold(I); electronic spectrum; TD-B3LYP

Introduction

The Au(I) complexes with intramolecular gold–gold interactions have been synthesized, characterized, and studied in detail, such as their absorption-emission spectrum [1–8]. Experimentally, the binuclear Au(I) compounds show a strong $^1(5d\sigma^* \rightarrow 6p\sigma)$ transition ultraviolet (UV)-visible attributed (singlet–singlet). The $5d\sigma^*$ assignment is refereed to the antibonding combination of $5d_{z2}(\sigma^*)$ orbitals and the $6p\sigma$ to the bonding combination $6p_z$ orbitals [9, 10]. The increase in energy of the $^1(5d\sigma^* \rightarrow 6p\sigma)$ transition for the Au(I) complexes can be explicable with a decreased in the Au–Au [$d(Au_2)$] distance, manifested as an increase in the vibrational frequency $\nu(Au_2)$ [3, 11]. The experimental data are shown in Table I for binuclear gold complexes.

The complexes studied in the present report show evidence of aurophilic interactions. Closed-shell aurophilic interactions (d^{10}–d^{10}) are estimated

Correspondence to: F. Mendizabal; e-mail: hagua@uchile.cl
Contract grant sponsor: Fondecyt/Conicyt (Chile).
Contract grant number: 1020141.

TABLE I

Experimental spectroscopic and structural values for selected compounds.*

System	λ $^1(d\sigma^* \rightarrow p\sigma)$	ν (Au_2)	d (Au_2)	Ref.
$[Au_2(dcpm)_2](ClO_4)_2$	277	88	292.6	1,2
$[Au_2(dmpm)_3](ClO_4)_2$	256	79	305.0	3
$[Au_2(dmpm)_2](Cl_2)$		71	301.0	3
$[Au_2(dmpm)_2](ClO_4)_2$	269	—	—	3
$[Au_2(dppm)_2](ClO_4)_2$	292	—	—	4
$[Au_2(CS_3)_2](^nBu_4N)_2$	314	125	279.9	5
$[Au_2(4,6\text{-}Me_2pym\text{-}2\text{-}S)_2]$	335	—	273.7	6

dcpm, bis(dicyclohexylphosphine)methane; dmpm, bis(dimethylphosphino)methane; dppm, bis(diphenylphosphino)-methane; CS_3, trithiocarbonate; 4,6-Me_2pym-2-S, 4,6-dimethylepyrimidinethiolate.

* Wavelengths λ in nm; frequency ν in cm^{-1}; distance in pm.

to be energetically similar to hydrogen bonds (20–50 kJ/mol) [12, 13]. At the theoretical level, the attraction is estimated when electronic correlation effects are taken into account, strengthened by relativistic effects [14, 15]. The mechanism behind such attraction is the dispersion (van der Waals) interaction, with additional allowance for virtual charge-transfer terms [16]. The optical properties of Au(I) complexes have been calculated from CIS and higher levels [17, 18]. Such properties have also been described efficiently with the density functional theory (DFT) with the time-dependent (DFT-TD) approach, makes it the method of choice. Several works have shown an excellent association with experimental absorption and emission spectrums [19–22].

The objective of the present work is to study theoretically the excitation spectra and vibrational frequency $\nu(Au_2)$ for complexes of the type $[Au_2(CS_3)_2]^{-2}$ (1), $[Au_2(pym\text{-}2\text{-}S)_2]$ (2) and $[Au_2(dpm)_2]^{+2}$ (3) at the B3LYP level. Thus far, no systematic DFT investigations have been carried in models 1 and 2. The complex $[Au_2(dpm)_2]^{+2}$ (3) has been studied by Zhang and Che [17] at the MP2 and CIS levels. In the present study, we have investigated model 3 by the B3LYP method, with the intention of comparing with the models 1 and 2.

Models and Methods

Models of the experimental structures $[Au_2(CS_3)_2]^{-2}$, $[Au_2(pym\text{-}2\text{-}S)_2]$ (pym = pyrimidethiolate), and $[Au_2(dpm)_2]^{+2}$ (dpm = bis(diphosphino)methane) used in our study are depicted in Figure 1. The dicyclohexylphosphine $[P(C_6H_5)_2]$, dimethylphosphino$[P(CH_3)_2]$ and diphenylphosphino(PPh_2) ligands of the original experimental structures are thereby replaced by the phosphine group (PH_3). In contrast, the ligand 4,6-dimethylepyrimidinethiolate (Me_2pym-2-S) is replaced by pyrimidethiolate (pym-2-S).

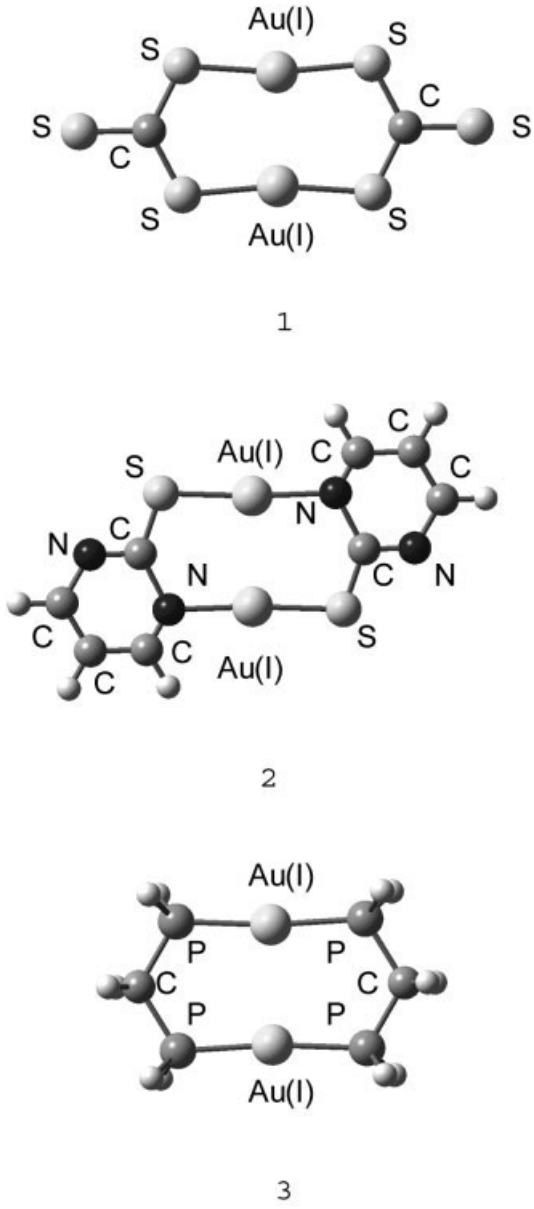

FIGURE 1. Binuclear gold(I) intramolecular models 1–3.

TABLE II

Main geometric parameters of models 1–3 (distances in pm and angles in degrees).

System	Method	Au–Au	Au–P	Au–S	Au–N	P–Au–P	S–Au–S	S–Au–N
$[Au_2(dcpm)_2](ClO_4)_2$	Exp.	292.6	231.8	—	—	173.9	—	—
$[Au_2(dmpm)_3](ClO_4)_2$	Exp.	305.0	236.4	—	—	178.0	—	—
$[Au_2(CS_3)_2](^nBu_4N)_2$	Exp.	279.9	—	230.0	—	—	172.8	—
$[Au_2(4,6\text{-}Me_2pym\text{-}2\text{-}S)_2]$	Exp.	273.7	—	226.4	210.2	—	—	176.0
$[Au_2(CS_3)_2]^{-2}(D_{2h})$ (1)	B3LYP	290.2	—	237.8	—	—	174.1	—
$[Au_2(pym\text{-}2\text{-}S)_2]$ (C_{2h}) (2)	B3LYP	269.2	—	229.5	221.0	—	—	175.8
$[Au_2(dpm)_2]^{+2}$ (C_{2h}) (3)	B3LYP	308.4	238.5	—	—	175.9	—	—

The geometries were fully optimized by the B3LYP method. Single-point calculations of these geometries were simulated to study the excitation spectra with TD-DFT and the gold–gold vibrational frequency $\nu(Au_2)$.

Calculations using the Gaussian 98 package were carried out [23]. The 19 valence–electron (VE) of the Au quasi-relativistic (QR) pseudo-potential (PP) of Andrae et al. [24] was employed. We used two *f*-type polarization functions on gold (α_f = 0.20, 1.19) [14]. Also, the C, P, N, and S atoms were treated through PPs, using double-zeta basis sets with the addition of one *d*-type polarization function [25]. For the H atom, a double-zeta basis set plus one *p*-type polarization function was used [26].

Energy excitation was obtained at the B3LYP level, using the time-dependent perturbation theory approach (TD-DFT) [27, 28], which is based on the random-phase approximation (RPA) method [29]. The TD-DFT approach provides an alternative to computationally demanding multireference configuration interaction methods in the study of excited states. TD-DFT calculations do not evaluate the spin-orbit splitting; the values are averaged.

The vibrational frequencies and force constants were computed by determining the second derivatives of the energy with respect to the Cartesian nuclear coordinates from the equilibrium geometry of each model.

Results and Discussion

MOLECULAR GEOMETRY

Table II presents the main parameters, together with relevant experimental structural data for binuclear gold(I) models 1–3. The theoretical results are in agreement with the experimental data. The gold–gold distance is mildly overestimated for model 1, but underestimated for model 2. However, the experimental trend is maintained.

These results should be analyzed with caution, since DFT calculations using B3LYP do not describe the aurophilic attraction correctly, although DFT can reproduce the distance metallophilic [30, 31]. The reason behind might be the specific form of the correlation energy, which is not adequately described [14–16]. Moreover, the B3LYP functional is able to mimic the process close to the gold–gold equilibrium distance [32]. Our goal is not to describe the aurophilic interaction and its magnitude, but the spectroscopic properties for the complexes mentioned.

TIME-DEPENDENT DENSITY FUNCTIONAL THEORY CALCULATIONS

We calculated the allowed spin singlet transition for these complexes, based on the ground-state structures of models 1–3. The objective was to evaluate the electronic structure of the excited state by direct electronic excitations. Only singlet–singlet transitions were considered in these quasi-relativistic calculations. The allowed transitions are shown in Figure 2 and are listed in Tables III–V. In the present study, we consider those transitions permitted whose oscillator strength is different from zero. The molecular orbitals (MOs) active in the electronic transitions are proved in Figures 3–5.

Model 1: $[Au_2(CS_3)_2]^{-2}$

This anion exhibits an experimental absorption spectrum with three characteristic bands [5]. The bands have been conventionally assigned as $n \rightarrow \pi^*$ (472 nm), $\pi \rightarrow \pi^*$ (384 nm) and $d\sigma^* \rightarrow p\ \sigma$ (314 nm). The two first bands are attributable to CS_3^{-2} local-

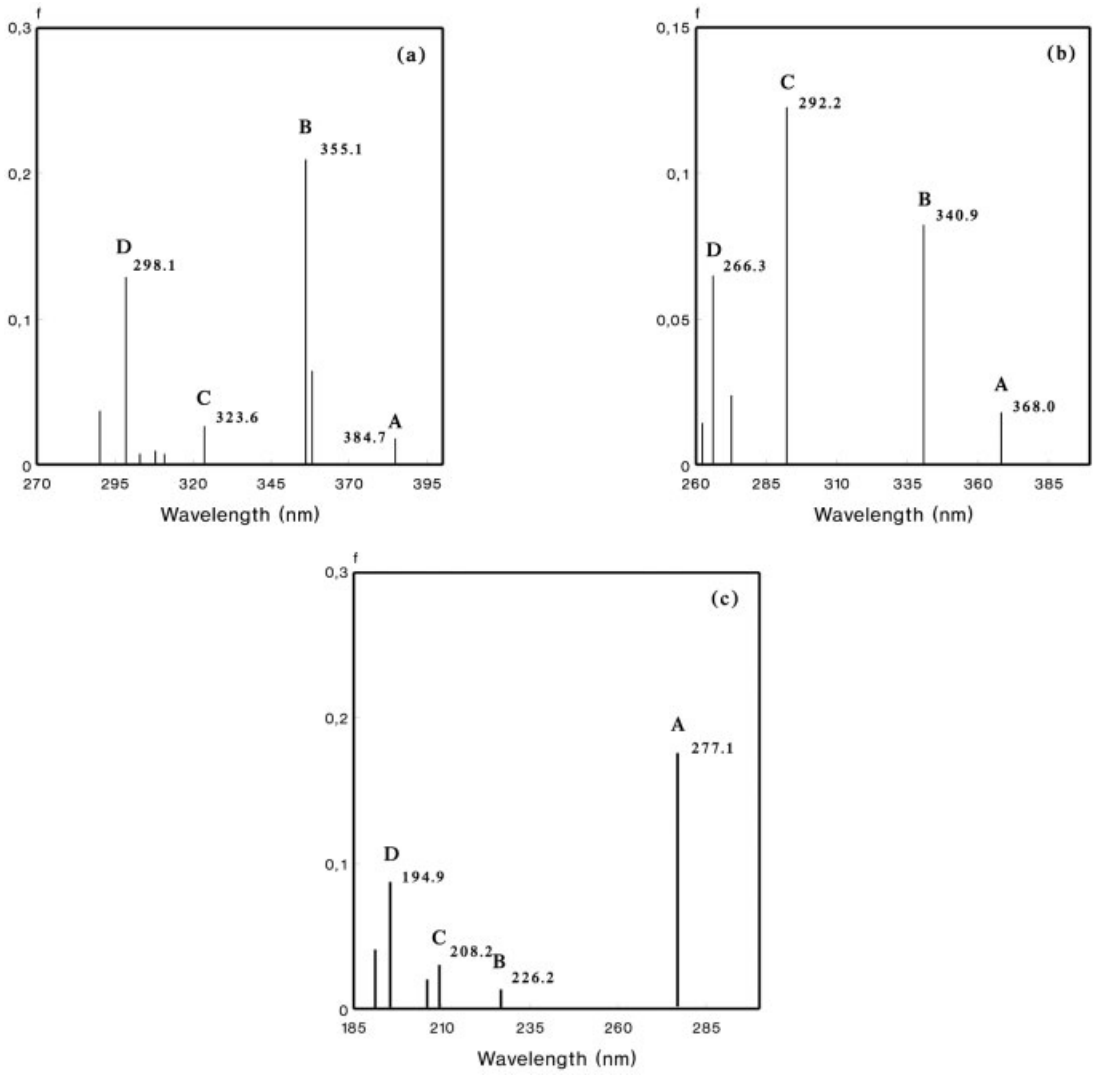

FIGURE 2. Calculated electronic spectrum: (a) $[Au_2(CS_3)_2]^{-2}$ (1), (b) $[Au_2(pym\text{-}2\text{-}S)_2]$ (2), (c) $[Au_2(dpm)_2]^{+2}$ (3).

ized transitions, while the last band is associated with a metal-centered (MC) gold(I)–gold(I) transition [5]. The theoretical calculations are described in Table III. The spectrum obtained is shown in Figure 2(a). There is good agreement with the experimental bands. We can observe that the theoretical excitations labeled A and B are related to the experimental spectrum. While B matches the experimental band, A does not agree because of the nature of the transition, $n \rightarrow \pi^*$, which is difficult on modeling. The bands at higher wavelengths are mainly $42b_{3g}$ $(n) \rightarrow 44b_{2u}$ $(d\pi^*)$ and $40b_{2g}$ $(\pi) \rightarrow 43b_{3u}$ (π^*), predominantly involving the C═S moiety, with little contribution of the metal. These bands correspond to ligand-to-ligand charge transfer (LLCT). The active molecular orbitals involved in the electronic transitions are shown in Figure 3.

We are interested in describing the 314 nm experimental band assigned as metal-centered charge transfer (MCCT) $5d_{z2}(\sigma^*) \rightarrow 6p(\sigma)$ [5]. The calculated transition at 298.1 nm (D) could be compared with the experimental band described above. This transition shows two principal components. First, the component with greater weight (47%) corresponds to $5d_{z2}(\sigma^*) \rightarrow 6p(\sigma)$ transition between the orbitals $41b_{2u}$ and $47a_g$, which we can understand from the OMs shown in Figure 3. The second component (23.4%) corresponds to a $36b_{1g}$ $(\pi^*) \rightarrow 43b_{3u}$ (π) transition attributable to the CS_3^{-2} ligand, which cannot be

TABLE III

TD-DFT/B3LYP singlet-excitation calculations for $[Au_2(CS_3)_2]^{-2}$.

Excitation	λ_{calc}/nm	f[a]	λ_{exp}/nm	ε[b]	Contributions[c]
A	384.7	0.0172	472	610	$42b_{3g} \rightarrow 44b_{2u}$ (72.2) $40b_{2g} \rightarrow 43b_{3u}$ (25.4)
B	358.1	0.0647	—	—	$41b_{2u} \rightarrow 45a_g$ (91.0) $39a_u \rightarrow 46b_{2g}$ (3.20)
B	355.1	0.2095	384	30680	$40b_{2g} \rightarrow 43b_{3u}$ (57.8) $42b_{3g} \rightarrow 44b_{2u}$ (25.8) $42b_{3g} \rightarrow 48b_{2u}$ (6.20)
C	323.6	0.0277	—	—	$41b_{2u} \rightarrow 47a_g$ (60.6) $39a_u \rightarrow 46b_{2g}$ (24.2) $36b_{1g} \rightarrow 43b_{3u}$ (4.98) $41b_{2u} \rightarrow 45a_g$ (3.20)
D	310.9	0.0056	—	—	$38b_{3u} \rightarrow 45a_g$ (95.8)
D	308.1	0.0109	—	—	$37b_{2u} \rightarrow 45a_g$ (83.6) $39a_u \rightarrow 46b_{2g}$ (9.00) $41b_{2u} \rightarrow 47a_g$ (2.60)
D	302.5	0.0071	—	—	$39a_u \rightarrow 46b_{2g}$ (43.6) $36b_{1g} \rightarrow 43b_{3u}$ (40.0)
D	298.1	0.1282	314	22250	$41b_{2u} \rightarrow 47a_g$ (47.0) $36b_{1g} \rightarrow 43b_{3u}$ (23.4) $39a_u \rightarrow 46b_{2g}$ (7.60) $37b_{2u} \rightarrow 45a_g$ (5.20) $37b_{2u} \rightarrow 47a_g$ (2.80)

[a] Oscillator strength.
[b] Experimental molar extinction coefficient in $dm^3\ mol^{-1}\ cm^{-1}$ in DMSO.
[c] Value is $|coeff.|^2 \times 100$.

TABLE IV

TD-DFT/B3LYP singlet-excitation calculations for $[Au_2(pym\text{-}2\text{-}S)_2]$.

Excitation	λ_{calc}/nm	f[a]	λ_{exp}/nm	ε[b]	Contributions[c]
A	368.10	0.0179	360	2750	$53a_u \rightarrow 56b_g$ (78.2) $52b_g \rightarrow 55a_u$ (12.4)
B	340.9	0.0822	335	5970	$52b_g \rightarrow 55a_u$ (81.4) $53a_u \rightarrow 56b_g$ (15.0)
C	292.2	0.1222	290	23270	$54b_u \rightarrow 59a_g$ (48.8) $53a_u \rightarrow 58b_g$ (40.6)
D	272.9	0.0243	—	—	$52b_g \rightarrow 57a_u$ (73.6) $53a_u \rightarrow 58b_g$ (21.8)
D	266.3	0.0648	—	—	$54b_u \rightarrow 59a_g$ (24.2) $54b_u \rightarrow 61a_g$ (21.8) $53a_u \rightarrow 58b_g$ (18.6) $49b_g \rightarrow 55a_u$ (12.4) $52b_g \rightarrow 57a_u$ (10.0) $52b_g \rightarrow 62a_u$ (2.40)
D	262.2	0.0138	—	—	$49b_g \rightarrow 55a_u$ (68.6) $54b_g \rightarrow 61a_g$ (29.0)

[a] Oscillator strength.
[b] Experimental molar extinction coefficient in $dm^3\ mol^{-1}\ cm^{-1}$ in DMSO.
[c] Values is $|coeff.|^2 \times 100$.

TABLE V

TD-DFT/B3LYP singlet-excitation calculations for $[Au_2(dpm)_2]^{+2}$.

Excitation	λ_{calc}/nm	f[a]	λ_{exp}/nm	ε[b]	Contributions[c]
A	277.1	0.1755	278	28920	$38a_g \rightarrow 39b_u$ (90.8)
B	226.2	0.0131	243	8846	$37b_u \rightarrow 39a_g$ (95.0)
C	208.2	0.0308	218	13000	$36a_g \rightarrow 40b_u$ (63.8)
					$31b_u \rightarrow 39a_g$ (32.6)
C	205.3	0.0205	—	—	$35b_g \rightarrow 40b_u$ (91.6)
D	194.9	0.0861	—	—	$38a_u \rightarrow 44b_g$ (40.0)
					$31b_u \rightarrow 39a_g$ (33.4)
					$36a_g \rightarrow 40b_u$ (14.0)
					$34a_u \rightarrow 44b_g$ (2.2)
					$28a_g \rightarrow 40b_u$ (2.12)

[a] Oscillator strength.
[b] Experimental molar extinction coefficient in $dm^3\ mol^{-1}\ cm^{-1}$ in acetonitrile for the complex $[Au_2(dcpm)_2](CiO_4)_2$.
[c] Values is $|coeff.|^2 \times 100$.

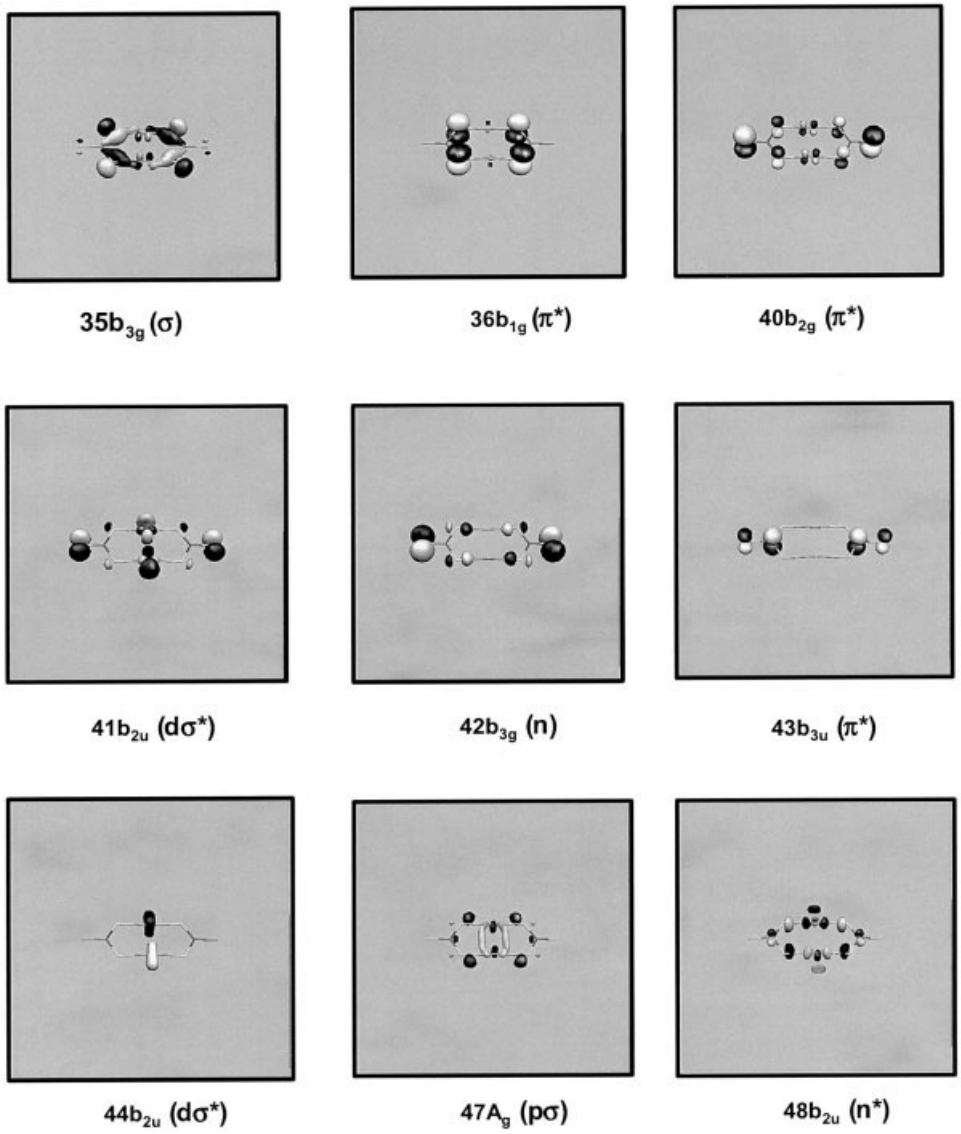

FIGURE 3. Molecular orbitals active in the electronic transitions $[Au_2(CS_3)_2]^{-2}$ (1).

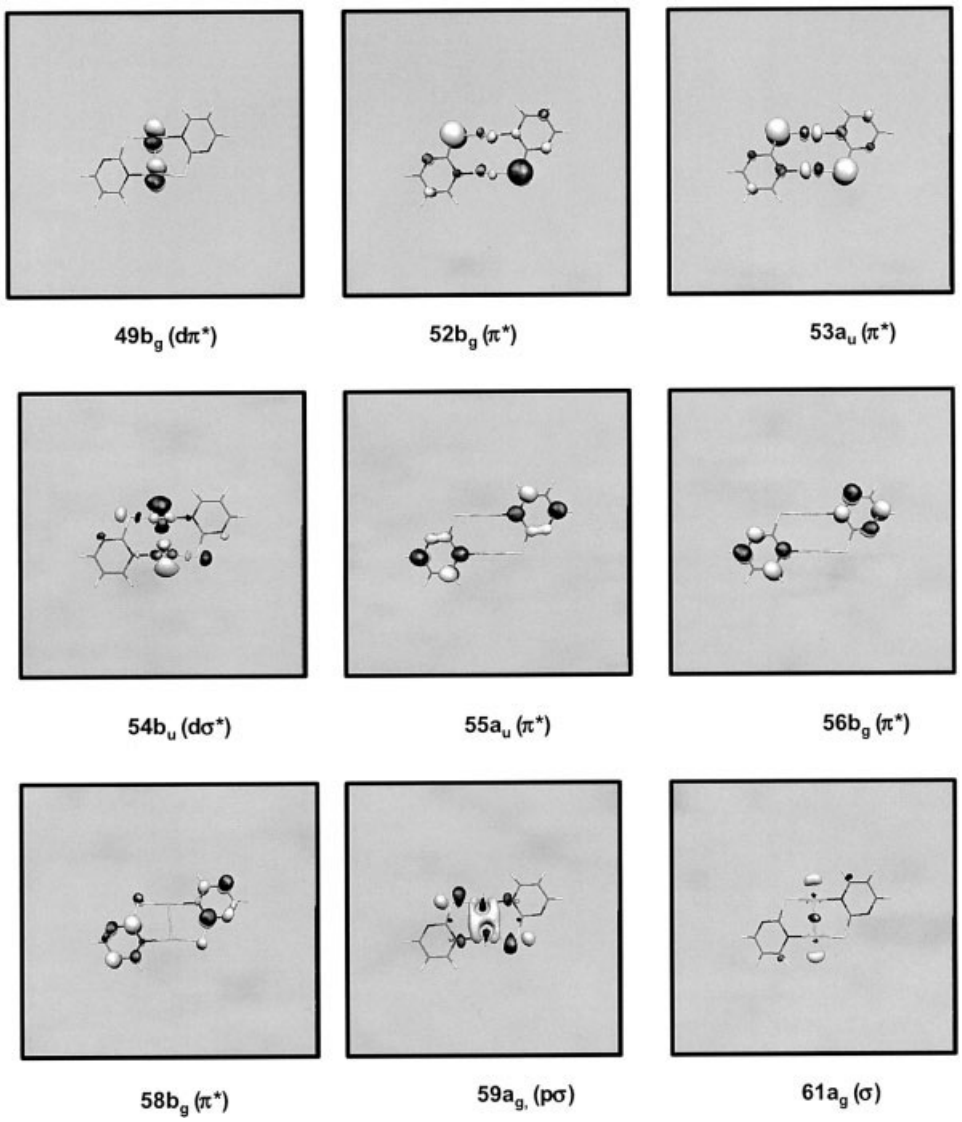

FIGURE 4. Molecular orbitals active in the electronic transitions [Au_2(pym-2-S)$_2$] (2).

despised due to the magnitude of its contribution. Thus, the electronics transition D is not MMCT pure.

Model 2: [Au_2(pym-2-S)$_2$]

In this model, the calculated singlet transition and the experimental wavelengths in [Au_2(4,5-Me_2pym-2-S)$_2$] [6] are presented in Table IV. The calculated spectrum is shown in Figure 2(b). The calculations show that the transitions at 368.10 nm (A), 340.9 nm (B), and 292.2 nm (C) match the experimental transitions at 360 nm, 335 nm, and 290 nm, respectively. At the experimental level, the absorption bands at 360 nm and 290 nm are attributed to LLCT, while the band at 335 nm is associated with a MCCT involving Au_2. At the theoretical level, we find a different interpretation. The bands at higher wavelengths (A and B) are mainly $53a_u$ (π^*) $\rightarrow$ $56b_g$ (π^*) and $52b_g$ (π) $\rightarrow$ $55a_u$ (π^*) involving predominantly the pym-2-S ligand, with little contribution of the metal. These bands correspond to LLCT. The MOs active in the electronic transition are shown in Figure 4.

The transition at 292.2 nm (C) in the theoretical spectrum is a mixture of the $54b_u \rightarrow 59a_g$ (48.8%) and $53a_u \rightarrow 58b_g$ (40.6%) excitations. The component with greater weight corresponds to a MCCT $5d_{z2}(\sigma^*) \rightarrow 6p(\sigma)$ (see MO in Fig. 4). The second component cor-

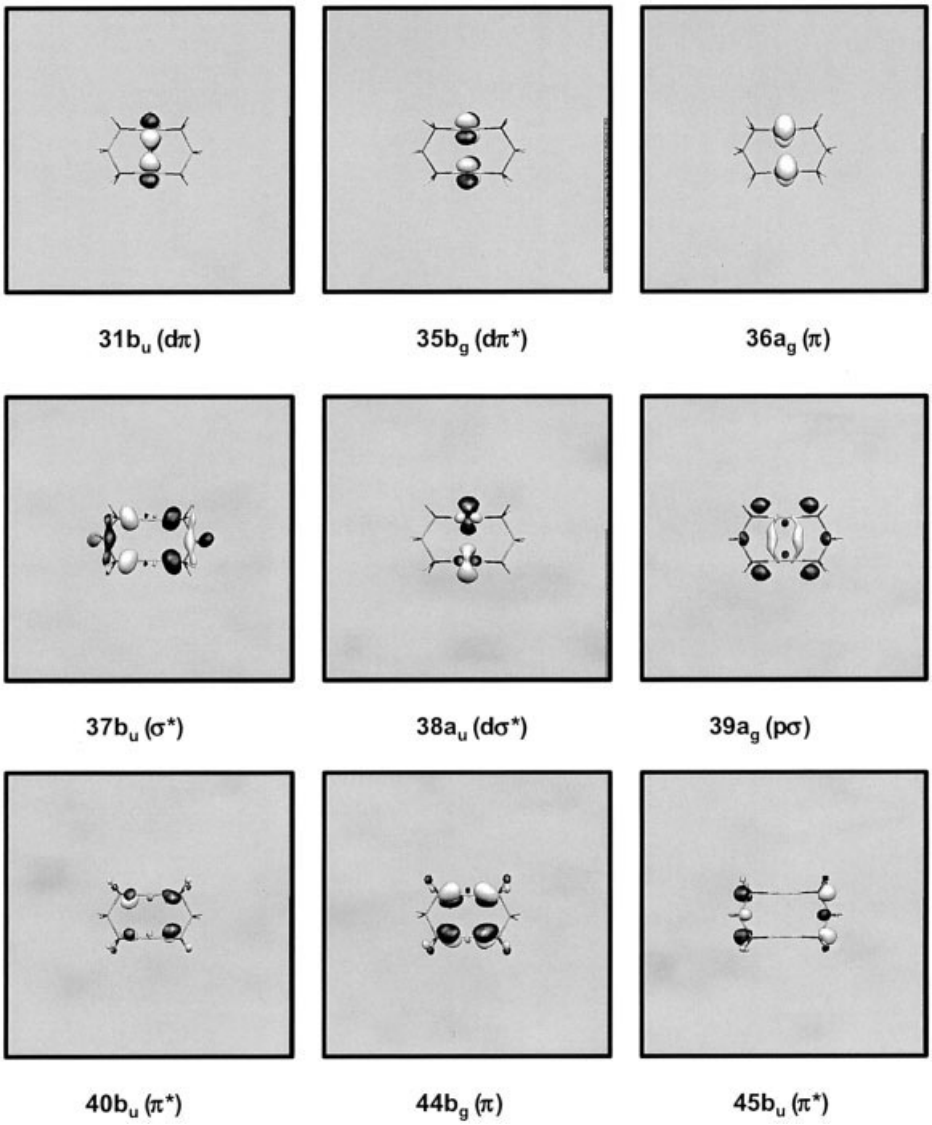

FIGURE 5. Molecular orbitals active in the electronic transitions $[Au_2(dpm)_2]^{+2}$ (3).

responds to a LLCT $\pi \rightarrow \pi^*$. Once again, the electronics transition is not MMCT pure. The LLCT component in C band is greater than in $[Au_2(CS_3)_2]^{-2}$ (1).

Model 3: $[Au_2(dpm)_2]^{+2}$

The theoretical transitions of the model system and experimental absorption spectroscopic data of the $[Au_2(dcpm)_2](ClO_4)_2$ [1, 2] are summarized in Table V and Figure 2(c). The experimental spectrum shows an intense absorption band at 277 nm, which is assigned to be the $5d_{z2}(\sigma^*) \rightarrow 6p(\sigma)$ transition. The calculated spectrum shows a theoretical transition A to 277.1 nm assigned as $38a_g \rightarrow 39b_u$, highest occupied molecular orbital–lowest unoccupied molecular orbital (HOMO–LUMO), (see Fig. 5), in excellent agreement with the experimental one. In a previous theoretical work, based on CIS calculations, Zhang et al. estimated using models that incorporate solvent molecules (acetonitrile) coordination with the gold atoms [17, 18], transition of 245.7 nm. Our calculations based on TD-DFT show a different behavior. It is not necessary to involve solvent molecules to describe the experimental spectrum and the MMCT bands.

The calculated transition at B (226.2 nm) and C (208.2 nm) may be compared with the experimental bands 243 and 218 nm, respectively. They correspond to theoretical transitions $37b_u \rightarrow 39a_g$ and $36a_g \rightarrow 40b_u$, associated mainly with LMCT and MLCT, respectively (see Fig. 5). There is reasonable agreement with the experimental bands.

MMCT DEPENDENCY WITH Au_2 DISTANCE

We have used models 1 and 3, $[Au_2(CS_3)_2]^{-2}$ and $[Au_2(dpm)_2]^{+2}$, respectively, to study the dependency of the MMCT band $[5d_{z2}(\sigma^*) \rightarrow 6p(\sigma)]$ with the distance Au_2. The reason for using both models is to analyze the effect of the change in the Au–Au distance and its impact on the MMCT band, which is pure in model 3, but not in model 1.

When the Au–Au distance changes from 350 to 250 pm, and the molecular symmetry and the remainders geometric parameters remain fixed, the absorption MMCT band varies from 313 to 278 nm (0.50 eV) and 276 to 316 nm (0.57 eV), by complexes 1 and 3, respectively. This result implies the variation of the distance among the gold atoms causes a red shift in the MMCT band. Figure 6 shows the correlation between the calculated MMCT band and the Au–Au distance. The nature in the composition of the band is largely maintained: $41b_{2u} \rightarrow 47a_g$ in model 1 and $38a_g \rightarrow 39b_u$ in model 3. The difference between both is the form of the curve, since model 1 shows a linear relationship and model 2 a decay. This indicated the importance of composition of the MMCT band.

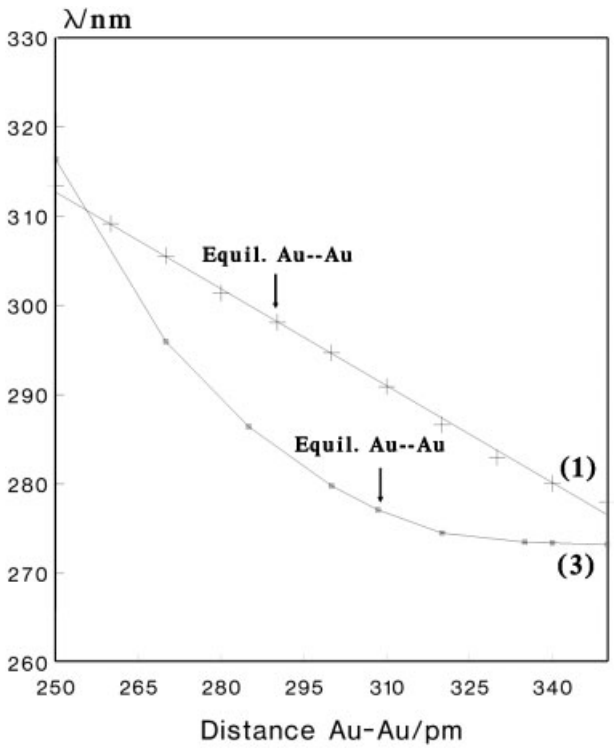

FIGURE 6. MMCT band dependency with gold–gold distance in models 1 and 2.

TABLE VI

Theoretical spectroscopic and structural values for models.*

System	$\nu(Au_2)$	F	$d(Au_2)$	λ $^1(5d_{z2}\sigma^* \rightarrow 6p\sigma)$
$[Au_2(dpm)_2]^{+2}$ (3)	70.4	0.2343	308.4	277.1
$[Au_2(CS_3)_2]^{-2}$ (1)	101.3	0.3455	290.2	298.1
$[Au_2(pym\text{-}2\text{-}S)_2]$ (2)	149.2	0.4407	269.2	292.2

dpm, bis(phosphine)methane; pym-2-S, pyrimidinethiolate.
* Frequency v in cm^{-1}; force constant F in mdyne/Å; distance in pm; wavelengths λ in nm.

It is evident that physical and chemical changes could have a significant effect on the distance among the gold atoms within the range of 270–310 pm, which would involve a shift in the MMCT band of the absorption spectrum. This conclusion may be appreciated in Table I for the experimental complexes.

VIBRATIONAL FREQUENCY $\nu(Au_2)$

We have carried out frequency calculations on models 1–3 at the B3LYP level for the ground state. No imaginary frequencies were found. Table VI presents the calculated Au–Au stretching frequency ($\nu(Au_2)$) and force constant (F), which are within the range of the experiment results (see Table I). Figure 7 shows each Au–Au stretching frequency of the ground state in models 1–3.

We have included the $^1(5d_{z2}\sigma^* \rightarrow 6p\sigma)$ theoretical transition and the gold–gold distance for comparison with the Au_2 stretching frequency. The decrease in gold–gold distance $d(Au_2)$ is related with increase in the frequency $\nu(Au_2)$ by $[Au_2(dpm)_2]^{+2}$, $[Au_2(CS_3)_2]^{-2}$ and $[Au_2(pym\text{-}2\text{-}S)_2]$, respectively. There is a good agreement between the experimental and theoretical parameters. In contrast, the increase in wavelength by MMCT in the systems shows less sensitivity with the decrease in $d(Au_2)$. This must be because, in models 1 and 2, the band associated with MMCT is not pure, as a second electronic transition associated with the ligands, which is not negligible.

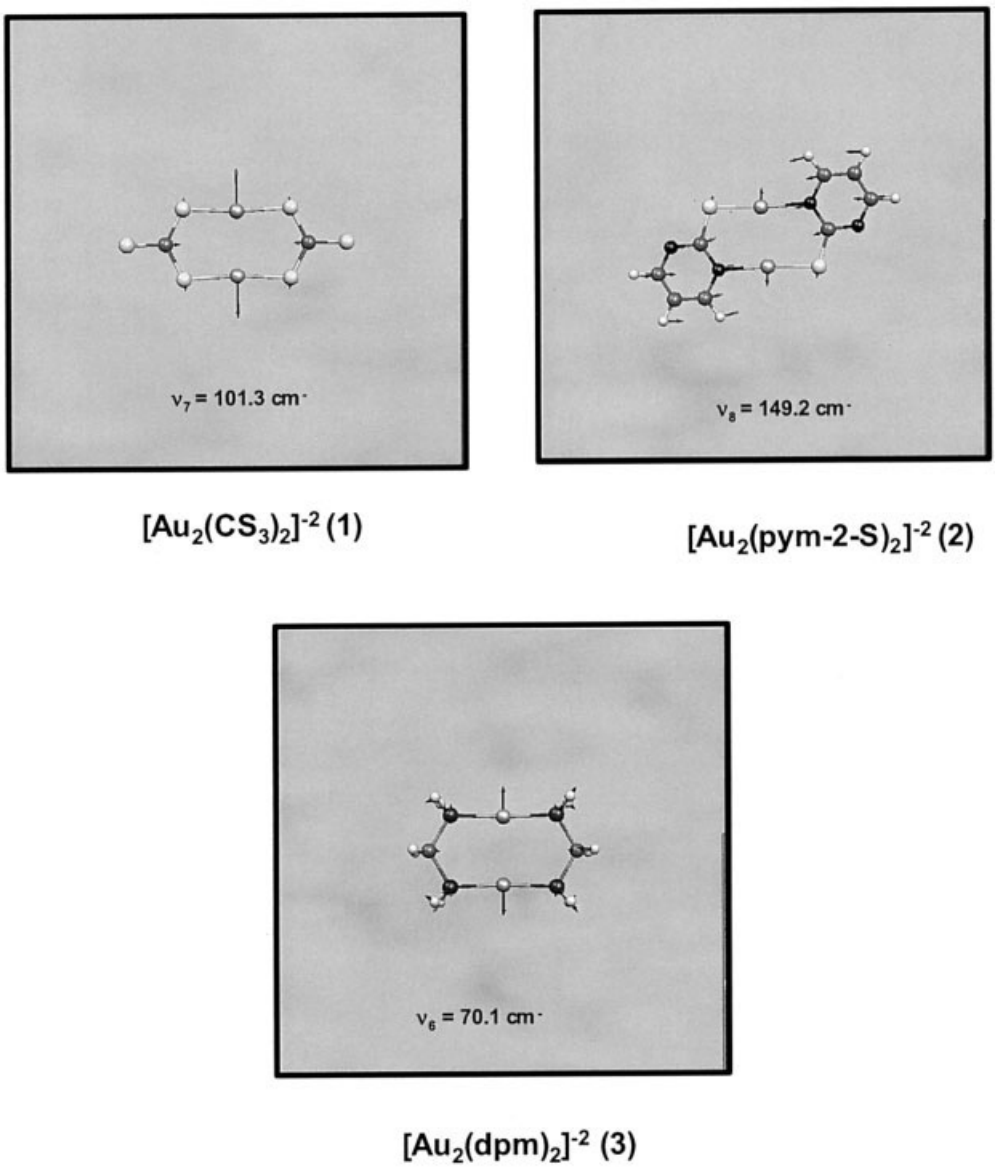

FIGURE 7. Au–Au stretching frequency in models 1–3.

Conclusions

We calculated spectroscopic properties, electronic spectrum, and vibrational frequency Au_2, for models 1–3 in the B3LYP version. It was demonstrated that it is possible to describe such properties according to the binuclear gold(I) complexes:

1. TD-DFT calculations match the experimental excitation spectrum. They show that intermetallic interactions are mainly responsible by the $^1(5d_{z2}\sigma^* \rightarrow 6p\sigma)$ MMCT.
2. In models 1 and 2, the theoretical transition associated with MMCT reveals the presence of a component LLCT. This could explain why this transition does not show a clear relationship with distance Au–Au.
3. There is a strong dependency between the Au–Au distance in each system and the MMCT band.
4. The Au–Au stretching frequency is correlated with the gold–gold distance, to greater frequency more short must be the distance Au–Au.

References

1. Fu, W.-F.; Chan, K.-C.; Miskowski, V. M.; Che, C.-M. Angew Chem Int Ed 1999, 38, 2783.
2. Leung, K. H.; Phillips, D. L.; Tse, M. C.; Che, C.-M.; Miskowski, V. M. J Am Chem Soc 1999, 121, 4799.
3. Leung, K. H.; Phillips, D. L.; Mao, Z.; Che, C.-M.; Miskowski, V. M.; Chan, C.-K. Inorg Chem 2002, 41, 2054.
4. Che, C.-M.; Kwong, H.-L.; Poon, C.-K. J Chem Soc Dalton Trans 1990, 3215.
5. Cheng, E.; Leung, K.-H.; Miskowski, V. M.; Yam, V. W.-W.; Phillips, D. L. Inorg Chem 2000, 39, 3690.
6. Hao, L.; Lachicotte, R. J.; Gysling, H. J.; Eisenberg, R. Inorg Chem 1999, 38, 4616.
7. King, C.; Wang, J.-C.; Khan, N. I.; Fackler, J. P., Jr. Inorg Chem 1989, 28, 2145.
8. Forward, J. M.; Bohmann, D.; Fackler, J. P., Jr.; Staples, R. J. Inorg Chem 1995, 34, 6330.
9. McCleskey, T. M.; Gray, H. B. Inorg Chem 1992, 31, 1733.
10. Che, C.-M.; Kwong, H.-L.; Yam, V. W.-W.; Cho, K.-C. J Chem Soc Chem Commun 1989, 885.
11. Perreult, D.; Drouin, M.; Michel, A.; Miskowski, V. M.; Schaefer, W. P.; Harvey, P. D. Inorg Chem 1992, 31, 695.
12. Pyykkö, P. Chem Rev 1997, 97, 597.
13. Schmidbaur, H. Gold Bull 2000, 33, 1.
14. Pyykkö, P.; Runeberg, N.; Mendizabal, F. Chem Eur J 1997, 3, 1451.
15. Pyykkö, P.; Mendizabal, F. Inorg Chem 1998, 37, 3018.
16. Pyykkö, P. Angew Chem Int Ed Engl 2002, 41, 1001.
17. Zhang, H.-X.; Che, C.-M. Chem Eur J 2001, 7, 4887.
18. Pan, Q.-J.; Zhang, H.-X. Eur J Inorg Chem 2003, 4202.
19. Fernández, E. J.; Gimeno, M. C.; Laguna, A.; López-deLuzuriaga, J. M.; Monge, M.; Pyykkö, P.; Sundholm, D. J Am Chem Soc 2000, 122, 7287.
20. Barone, V.; Fabrizi de Biani, F.; Ruiz, E.; Sieklucka, B. J Am Chem Soc 2001, 123, 10742.
21. Fernández, E. J.; Jones, P. G.; Laguna, A.; López-de-Luzuriaga, J. M.; Monge, M.; Pérez, J.; Olmos, M. E. Inorg Chem 2002, 41, 1056.
22. Fernández, E. J.; Laguna, A.; López-de-Luzuriaga, J. M.; Mendizabal, F.; Monge, M.; Olmos, M. E.; Pérez, J. Chem Eur J 2003, 9, 456.
23. Frisch, M. J.; Trucks, G. W.; Schlegel, H. B.; Gill, P. M. W.; Johnson, B. G.; Robb, M. A.; Cheeseman, J. R.; Keith, K. T.; Petersson, G. A.; Montgomery, J. A.; Raghavachari, K.; Al-Laham, M. A.; Zakrzewski, V. G.; Ortiz, J. V.; Foresman, J. B.; Cioslowski, J.; Stefanov, B. B.; Nanayakkara, A.; Challacombe, M.; Peng, C. Y.; Ayala, P. Y.; Chen, W.; Wong, M. W.; Andres, J. L.; Replogle, E. S.; Gomperts, R.; Martin, R. L.; Fox, D. J.; Binkley, J. S.; Defrees, D. J.; Baker, J.; Stewart, J. P.; Head-Gordon, M.; Gonzalez, C.; Pople, J. A. Gaussian 98, Revision A.11; Pittsburgh, PA, 2002.
24. Andrae, D.; Häusserman, U.; Dolg, M.; Stoll, H.; Preuss, H. Theor Chim Acta 1990, 77, 123.
25. Bergner, A.; Dolg, M.; Küchle, W.; Stoll, H.; Preuss, H. Mol Phys 1993, 80, 1431.
26. Huzinaga, S. J Chem Phys 1965, 42, 1293.
27. Bauernschmitt, R.; Ahlrichs, R. Chem Phys Lett 1996, 256, 454.
28. Casida, M. E.; Jamorski, C.; Casida, K. C.; Salahub, D. R. J Chem Phys 1998, 108, 4439.
29. Olsen, L.; Jørgensen, P. In Modern Electronic Structure Theory, Vol. 2; Yarkony, D. R., Ed.; World Scientific: River Edge, NJ, 1995.
30. Wang, S.-G.; Schwarz, W. H. E. J Am Chem Soc 2004, 126, 1266.
31. O'Grady, E.; Kaltsoyannis, N. Phys Chem Chem Phys 2004, 6, 680.